JOURNAL OF PROPULSION AND POWER
Vol. 23, No. 4, July–August 2007

# Atomization and Flames in $LOX/H_2$- and $LOX/CH_4$-Spray Combustion

Baoe Yang*
*Northwestern Polytechnical University, 710072 Xi'an, People's Republic of China*
Francesco Cuoco†
*Avio S.P.A., 00034 Colleferro, Italy*
and
Micale Oschwald‡
*Institute of Space Propulsion, 74239 Hardthausen, Germany*

DOI: 10.2514/1.26538

**Hydrogen is a widely used rocket fuel and methane is particularly of interest in Europe as a promising substitute for $H_2$. Experimental investigation of cryogenic reactive coaxial sprays with oxygen as an oxidizer and hydrogen and methane as fuels is conducted to prove whether concepts from the $LOX/H_2$ injector design can be transferred to $LOX/CH_4$ injection. The liquid oxygen has been atomized in shear coaxial atomizers, and the sprays and flames have been investigated by visualization methods such as shadowgraphy and imaging of the flame emission. LOX sprays are characterized for both propellants by the intact core lengths and droplet numbers, and the combustion is analyzed in terms of the flame anchoring mechanism and the flame spreading angle. The results for $LOX/H_2$- and $LOX/CH_4$-spray combustion are compared, and the influence of the injection conditions of the propellants on atomization and spray flame is discussed. Significant differences of the sprays and flames have been observed for the two propellant combinations at similar injection conditions, as defined by the Weber number and the momentum flux ratio. The flame stabilization process has shown a strong influence on the atomization and flame characteristics.**

## Nomenclature

| | | |
|---|---|---|
| $a$ | = | thermal diffusivity |
| $d, D$ | = | diameter |
| $J$ | = | gas-to-liquid momentum flux ratio, $J = (\rho u^2)_g/(\rho u^2)_l$ |
| $L$ | = | intact liquid core length |
| $Oh$ | = | Ohnesorge number, $Oh = \mu_l/\sqrt{\sigma \rho_l d_l}$ |
| $Re$ | = | Renolds number, $Re = \rho u d/\mu$ |
| $Rv$ | = | gas-to-liquid velocity ratio, $R_V = u_g/u_l$ |
| $S$ | = | flame speed |
| $t$ | = | LOX post thickness |
| $u$ | = | velocity |
| $We$ | = | Weber number based on relative velocity, $We = \rho_g(u_g - u_l)^2 d_l/\sigma$ |
| $\delta$ | = | flame thickness |
| $\mu$ | = | viscosity |
| $\rho$ | = | density |
| $\sigma$ | = | surface tension |

*Subscripts*

| | | |
|---|---|---|
| $F$ | = | flame |
| $f$ | = | fuel |
| $g$ | = | gas |
| $L$ | = | laminar |
| $l$ | = | liquid |
| $o$ | = | oxygen |

Received 14 July 2006; revision received 31 January 2007; accepted for publication 4 February 2007. 

*Ph.D. Candidate, College of Astronautics, PO Box 15-11, 710010 Xi'an.
†Ph.D. Candidate, Space Propulsion.
‡Doctor, Head of Rocket Propulsion, DLR Lampoldshausen. Member AIAA.

## I. Introduction

HYDROGEN is widely used as the fuel of liquid rocket engines because it delivers the highest specific impulse compared to other fuels, including hydrocarbons. This advantage of $H_2$, however, is compromised in part by other performance characteristics as, for example, its cryogenic and low-density properties, costs, and difficulty of handling. Other noncryogenic propellants like the hypergolic MMH/NTO are toxic where nontoxic propellant substitutes are most desirable. For this reason hydrocarbons have come into focus in Europe as fuels for rocket propulsion, among these, $CH_4$ and kerosene are particularly of interest. The main advantages of using hydrocarbons are the high propellant density, reduced handling effort, and reduced safety precautions.

Propellant injectors are key components controlling liquid fuel atomization, mixing, combustion, and thus by a major part efficiency and stability of combustion in rocket engines. For $LOX/H_2$ combustion chambers, the standard injection element is the shear coaxial injector as shown in Fig. 1. Liquid oxygen is injected through the central tube and the gaseous fuel through the annular slit.

The atomization in coaxial injection is due to a complex interaction of several forces. Turbulence in the liquid jet as well as the adaptation of its velocity profile to the new boundary conditions when the liquid jet leaves the injector may result in distortions of the liquid jet surface. These surface distortions which are amplified by aerodynamic forces of the high-speed annular gas flow, along with liquid jet destabilization, will result in final jet disintegration. Viscosity and inertia of the liquid have damping effects on the disintegration dynamics. Because of the complexity of the disintegration the basic mechanisms leading to atomization are neither completely identified nor well modeled [1]. Therefore the design of injectors is mainly based on empirical correlations that use nondimensional parameters characterizing the relative importance of the contributing forces. These nondimensional numbers are formed from the geometrical characteristics of the injector and the fluid-dynamic properties of the propellants. Most prominent in this context are the Weber number, the ratio of the aerodynamic force to the surface tension,

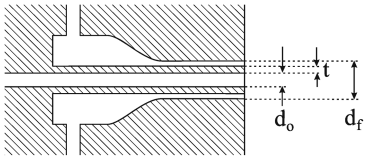


**Fig. 1 Sketch of a coaxial injector.**

$$We = \frac{\rho_g (u_g - u_l)^2 d_l}{\sigma}$$

and the momentum flux ratio

$$J = \frac{(\rho u^2)_g}{(\rho u^2)_l}$$

The Weber number was used by Farago and Chigier [2] to classify the atomization process according to morphology of the disintegrating liquid jet. They found that the Weber number controls whether the atomization process is in the Rayleigh breakup regime ($We < 25$), and it shows a membrane-type breakup ($25 < We < 100$) or a fiber-type breakup ($100 < We < 500$). Based on water/air experiments Engelbert et al. [3] pointed out the influence of the local Weber number on the droplet size instead of the Weber number in the injector exit plane. These experiments further showed the influence of the momentum flux ratio on the breakup length. Lasheras et al. [4] derived for the dependence of the breakup length $L$ on $J$:

$$\frac{L}{d_l} \approx \frac{6}{\sqrt{J}} \tag{1}$$

Recent research on coaxial jet breakup lengths conducted by Davis [5] and Woodward et al. [6] showed considerably longer breakup lengths than predicted by the above correlation of Lasheras et al. The correlation derived by Davis from cold-flow experiments for two-phase coaxial jets was

$$\frac{L}{d_l} = \frac{25}{J^{0.2}} \tag{2}$$

For single-phase coaxial jets in supercritical regime:

$$\frac{L}{d_l} = \frac{12}{J^{0.5}}$$

Woodward et al. suggested a $\ell_n(J)$ scaling for correlating the LOX dense core length from their limited $LOX/H_2$ hot fire data at supercritical conditions.

There are other nondimensional groups related to liquid jet atomization, for instance, the velocity ratio, the Ohnesorge number, and the liquid Reynolds number. The velocity ratio $R_V = u_g/u_l$ had been found in experiments to be a nondimensional group characterizing $LOX/H_2$-spray flames in respect to combustion stability [7] or combustion efficieny [8]. Drop breakup regimes in cold flows [9,10] have been classified by the Ohnesorge number $Oh = \mu_l/\sqrt{\sigma \rho_l d_l}$. As a ratio of inertial and viscosity, liquid jet Reynolds number may also play a role in jet disintegration as Eroglu and Chigier [11] observed for airblast coaxial atomizers at low Weber number ($We < 300$).

The relative importance of the forces involved in the atomization process strongly depends on the injection conditions, the physical properties of the propellants, and the local flowfield in the spray. This is the reason why even in nonreacting sprays correlations derived from experimental results only show a rough agreement, for example, there are inconsistencies on which property increases or decreases droplet size [8]. An extrapolation of correlations obtained in cold-flow tests with water to cryogenic conditions with the low level of surface tension and viscosity of liquid oxygen is therefore highly unreliable. This is due to the fact that the Reynolds numbers of liquid oxygen are generally 1 order of magnitude below representative conditions ($Re \approx 10^5$–$10^6$) when using substitute fluids such as water.

For cold-flow coaxial injection, there are numerous experimental and theoretical investigations [1–5,10–16]. The major question, however, is whether and how results from cold-flow tests can be transferred to hot fire conditions. Unfortunately there are not very much data with systematic parameter variation for reactive sprays available. In Fig. 2, an image of the emission of the OH radical in the flame of coaxial $LOX/H_2$ spray is shown. It is clearly seen that the flame is stabilized in the wake of the rim of the central LOX tube, also known as LOX post. As a consequence, the LOX jet is separated from the annular $H_2$ high-speed gas flow by the reaction front and a turbulent mixing layer of hot reaction products and reactants. Combustion in hot fire tests has therefore several consequences for the atomization process.

For an attached flame, the liquid oxygen jet is not directly exposed to the aerodynamic forces of the annular gaseous fuel flow, but these forces have to be transmitted by the turbulent mixing layer to the liquid surface. As a consequence the spray formation may happen under a different atomization regime as compared to cold-flow conditions. Visualization of LOX sprays at identical injection conditions in cold flow and hot fire tests for instance clearly shows the faster evaporation of the small LOX droplets in the reactive flow.

From this discussion, the limitations of cold-flow tests in predicting hot fire atomization become evident. When discussing the role of the fuel properties on the atomization process it is not enough to focus only on the physical properties of the fuel like its density, injection velocity, etc., but the kinetic properties of the reaction partners, and the turbulent transport properties have to be taken into account as well.

Flame anchoring at the LOX post as shown in Fig. 2a has been consistently observed for $LOX/H_2$ injection [17–20]. However with a different fuel type such as $CH_4$, a lifted flame anchoring in the turbulent mixing layer of evaporated LOX and gaseous fuel is also a possible flame anchoring mechanism (see Fig. 2b). In this case the interaction of combustion with the spray formation process starts downstream of the flame anchoring position. Juniper and Candel [21] derived from numerical investigations that the nondimensional quantity $\psi = t/\delta_F$, the ratio of LOX-post thickness $t$ and the flame thickness $\delta_F$, is a control parameter for the flame stabilization behavior.

There is a huge database on $LOX/H_2$ combustion in Europe. It is worthwhile then to compare $LOX/CH_4$- to $LOX/H_2$-spray

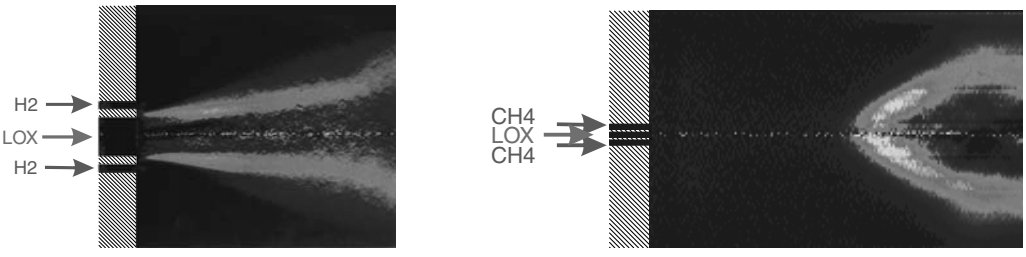


**a) $LOX/H_2$-flame anchored at the LOX-post** **b) Lifted flame anchoring in the $O_2/CH_4$ shear layer**

**Fig. 2 Different flame anchoring mechanisms. Shown is the imaging of OH emission a) observed in a model combustor at the test bench P8 of DLR (German Aerospace Center), and b) this work.**

**Table 1 Thermophysical properties of propellants at injector exit conditions of this paper: $P = 0.15$ MPa, $T = 80$ K for LOX and $H_2$, ambient temperature for $CH_4$ [22,23]**

| | $O_2$ | $CH_4$ | $H_2$ |
|---|---|---|---|
| Critical temperature, K | 154.6 | 190.5 | 32.9 |
| Critical pressure, MPa | 5.04 | 4.60 | 1.28 |
| Reduced pressure, $P/P_{crit}$ | 0.030 | 0.033 | 0.12 |
| Reduced temperature, $T/T_{crit}$ | 0.52 | 1.51 | 2.43 |
| Density, $kg/m^3$ | —— | 1.01 | 0.456 |
| Viscosity, $\mu Pa \cdot s$ | —— | 10.86 | 3.57 |
| Specific heat, $J/kg \cdot K$ | —— | 2213 | 10,766 |
| Thermal conductivity, $W/m \cdot K$ | —— | 0.0329 | 0.0566 |
| Thermal diffusivity, $10^{-5}$ $m^2/s$ | —— | 1.47 | 1.15 |
| Laminar flame velocity @ ambient [24], m/s | —— | 3.93 | 10.7 |
| Ignitability limits [25], Vol % | —— | 5.1–61 | 4–94 |

**Table 2 Injector geometries and test conditions**

| | $LOX/H_2$ injector | | $LOX/CH_4$ injector |
|---|---|---|---|
| LOX-post inner diameter $d_o$, mm | 1.2 | 1.6 | 1.4, 1.6 |
| LOX-post thickness $t$, mm | 0.4 | | 0.4 |
| Annular slit diameter $d_f$, mm | 4.8, 5.2, 5.7 | 4.9, 5.7, 6.9 | 5.0, 5.7, 6.9 |
| LOX inlet temperature, K | 80 | | 80 |
| Fuel inlet temperature, K | 80 | | Ambient temperature |
| LOX mass flow rate, g/s | 8–20 | | 11–24 |
| Propellant mixture ratio | 5.5 | | 3.4 |
| Combustion pressure, MPa | 0.15 | | 0.15 |

combustion to prove whether concepts from $LOX/H_2$-injector design can be transferred to $LOX/CH_4$ injection. Comparing the thermophysical properties it can be assumed that there may be limitations. Some properties of the propellants at the test conditions of this paper are listed in Table 1 where differences can be identified. At the injection conditions the density of methane is more than 2 times the density of $H_2$ and the specific heat only about 0.2 times that of $H_2$ at typical injection conditions. The combination of these properties shows the impact on the flame through thermal diffusivity. The flame thickness $\delta_F$ is related to the laminar flame speed $S_L$ and the thermal diffusivity $a$ by the following equation: $\delta_F = 2a/S_L$ [26]. The laminar flame speed for $CH_4/O_2$ is about a factor of 2.5 below the value for $H_2/O_2$, which may be of great importance for flame propagation and stabilization during the ignition transient and flame anchoring phenomenology at stationary conditions. And the remarkable difference in ignitability in the fuel rich limit has to be pointed out.

The experimental work presented in this paper is dedicated to show the influence of the fuel properties and its kinetics on atomization and combustion by comparing $LOX/CH_4$- and $LOX/H_2$-spray combustion phenomenology.

## II. Test Setup

### A. Test Bench and Combustor

The experimental investigation had been performed on the M3 test facility at DLR-Lampoldshausen, Germany. The test bench is equipped with a single-injector combustion chamber (see Fig. 3) with $140 \times 40$ mm$^2$ quartz windows for optical access for visualizing the spray and flame development. Combustion can be initiated in two ways: a torch igniter or Nd:YAG-laser induced plasma. The latter method produces precise ignition energy, timing, and positioning. Propellants mass flow rates were chosen to achieve 0.15 MPa combustion chamber pressure once steady-state conditions are reached. The duration for each test was 2 s because the optical windows were uncooled. The Weber and $J$-number combinations were varied in the investigation from 500–16,000 and from 0.2 to 2.0, respectively, via changing the LOX post and faceplate geometry of the coaxial injector. The main parameters of injector geometries and test conditions were summarized in Table 2. To check the experimental reproducibility, at least two tests were conducted for one experimental test case.

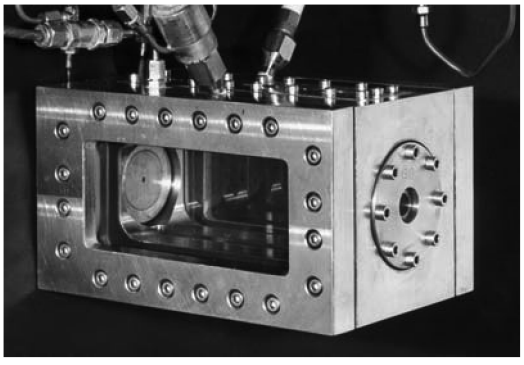

**Fig. 3 The M3 combustor.**

The experimental conditions are representative of real engines in respect to the temperature of the cryogenic propellants. Regarding the $J$ and Weber numbers, the experiments reflect the lower boundaries of representative conditions for $LOX/H_2$-rocket combustors. The chamber pressure, limited to 0.15 MPa in these tests by the experimental setup, mainly influences the surface tension of liquid oxygen and the coaxial gas density. In spite of the chamber pressure limitation, the results presented may help to understand the interaction between atomization and flame characteristics and to prove whether concepts from $LOX/H_2$-injector design can be transferred to $LOX/CH_4$ injection.

### B. Flow and Flame Visualization Techniques

A high-resolution shadowgraph setup was used for obtaining the liquid oxygen spray information. Shadowgraphs have been recorded using a Kodak Flowmaster 2k camera with a high spatial resolution of 0.055 mm/pixel and 4 frames/s acquisition rate. The flowfield was "frozen" by means of a back light from a nanolite with a 18 ns flash duration.

Flame development was visualized with an intensified high-speed charge-coupled device (CCD) camera with a 9 kHz acquisition rate and a $256 \times 128$ pixel resolution. The camera was fitted with a UV lens and a narrowband filter (300–310 nm) to record the OH-radical emission during the combustion process.

## III. Data Reduction

### A. Spray Information from Shadowgraph Images

#### 1. *Liquid Intact Core Length*

Liquid intact core length, which is also called "breakup length" or "decay length," refers to the distance from an injector exit surface to the point a continuous jet breaks up. This is the most straightforward spray information that can be extracted quantitatively from shadowgraph images. Images are processed as shown in Fig. 4 by converting an intensity image into a binary image and labeling the disconnected components as different objects. The most upstream object is taken as the liquid intact core.

The dependence of intact core length determination on the threshold value has been tested on three typical images as shown in Fig. 5. If the threshold value is chosen to be too small, bright liquid is identified as background, and hence the evaluated core length would be too small. If the threshold is too high, then the evaluated intact core length will be too large. The threshold value is the most critical parameter in the process of intact core length determination. There exists a threshold range in which the discrimination between liquid and background is not sensitive to the threshold. In Fig. 5 the intact core lengths determined from one image vary less than 3% for a

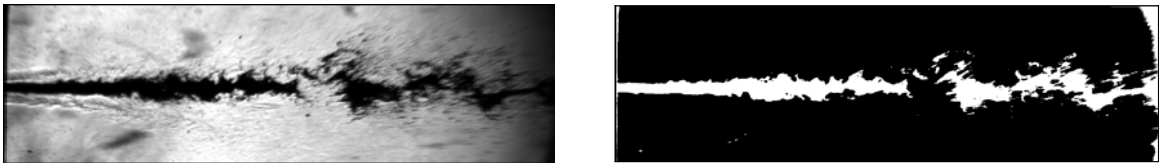

**a) Intensity image (LOX/$H_2$, *We*=9844, *J*=1.28)** **b) Binary image**

**Fig. 4 Processing of shadowgraph images for liquid intact core length.**

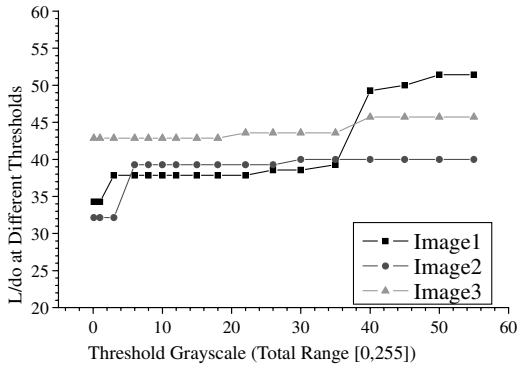


**Fig. 5 Effect of thresholds on determination of liquid intact core length.**

variation of the threshold level between 10 and 35. The specific threshold for each test condition has been chosen individually depending on the image characteristics and is typically in the range of 25–30.

During stationary flow conditions the length of the intact core varies due to the intrinsic instability of the liquid jet atomization process. The variation of the core lengths evaluated from different images in one test is therefore much higher than the error due to the chosen threshold level. For instance, the standard deviation of the intact core lengths measured in one test at conditions of Fig. 4 is 20.3% of the mean but the error from thresholds is less than 3% as mentioned above.

*2. Liquid Droplet Number*

The objective of liquid jet atomization is to break up a jet into droplets as fine as possible to maximize the liquid surface area. Although we cannot get droplet sizes from shadowgraph images, numbers of droplets discernible in the shadowgraph images may be counted as a quantitative way to characterize the atomization process.

The raw images have to be converted into binary images to label droplets, including the jet itself and other large liquid structures, as different objects. The results are more sensitive to image processing as compared to the determination of the liquid core length. Droplets have to be discriminated against the background in a much larger image area with a variation of the background level as compared to the liquid intact core. Contrast enhancement has been done on image subareas which then have been converted into binary images (see the top images of Fig. 6). The subareas and the threshold level have been tuned by the operator's judgment so that the binary images reflect the main information observed in the original image. Droplet numbers obtained by this process appeared to vary by about 12% in the selected threshold range. The major contribution to this error originates from the image noise.

Because of the spatial resolution limitation (55 $\mu$m) of the shadowgraph images, only drops at least larger than 1–2 pixel size can be identified. This introduces systematic errors in the determination of droplet numbers. At the same time, the discernible drops are very different in their sizes and this information of atomization cannot be reflected by the droplet numbers. With these limitations in mind a qualitative comparison of the results obtained in different tests is done. Although the droplet-number information is only a rough statistic of the atomization process it appeared to be very effective in analyzing the Weber and *J* effects on atomization as shown in the next section.

### B. Flame Information from OH Images

OH-emission images have been processed to obtain the flame spreading angle. A flame angle is estimated from the average of OH images in one test run. The flame boundary is determined by separating the flame from the background by using an adequate threshold to remove image noise such as signals due to reflection from the combustor walls (see Fig. 7). Two lines are fitted to the boundary of the conical flame surrounding the LOX spray. Half of the angle between these two lines represents the flame spreading angle. Based on the sensitivity of the spreading angle on varying the threshold in the grayscale range of 45–55, we estimated an accuracy of about 4% of the angle.

## IV. Results and Analysis

### A. Sprays

*1. Qualitative Comparison of Sprays in* $LOX/H_2$ *and* $LOX/CH_4$ *Hot Fire Tests*

As shown in Figs. 8–10, liquid oxygen sprays behave very differently in $LOX/H_2$ and $LOX/CH_4$ hot fire tests. If coaxial spray atomization is mainly controlled by the dimensionless numbers

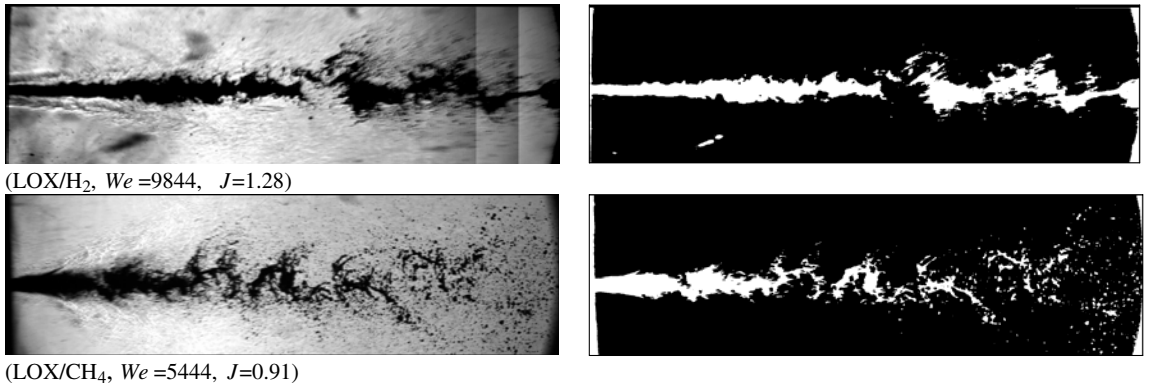

($LOX/H_2$, *We* =9844, *J*=1.28)

($LOX/CH_4$, *We* =5444, *J*=0.91)

**a) Processed intensity image** **b) Binary image**

**Fig. 6 Processing of shadowgraph images for droplet numbers.**

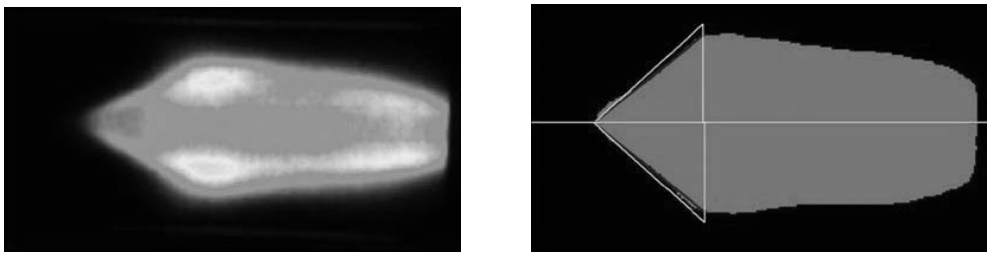

a) Average image of the flame b) Flame angle calculation

**Fig. 7 Processing of OH images for flame angles.**

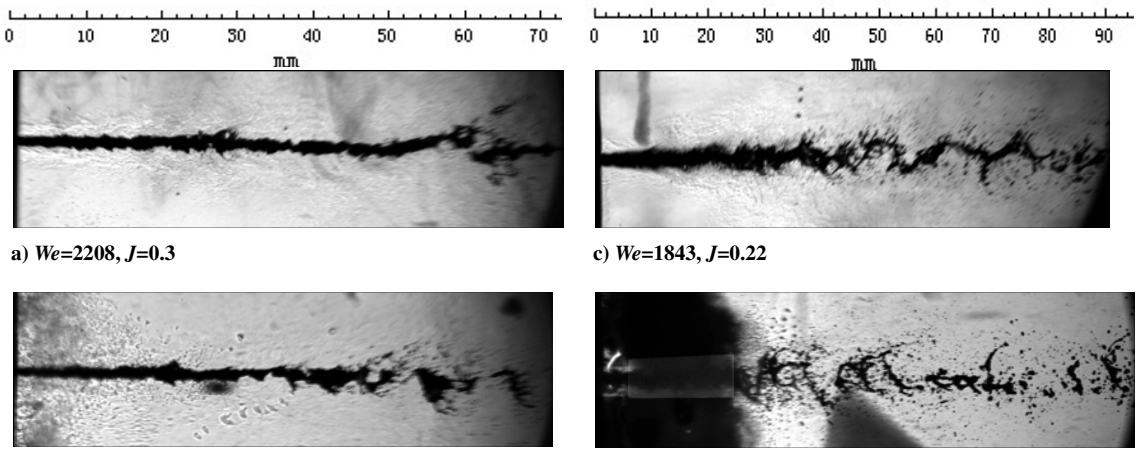


a) *We*=2208, *J*=0.3 c) *We*=1843, *J*=0.22

b) *We*=2462, *J*=0.73 d) *We*=2498, *J*=0.95

**Fig. 8 *J* effect at the Weber number around 2000 for a), b) $LOX/H_2$ tests, and c), d) $LOX/CH_4$ tests.**

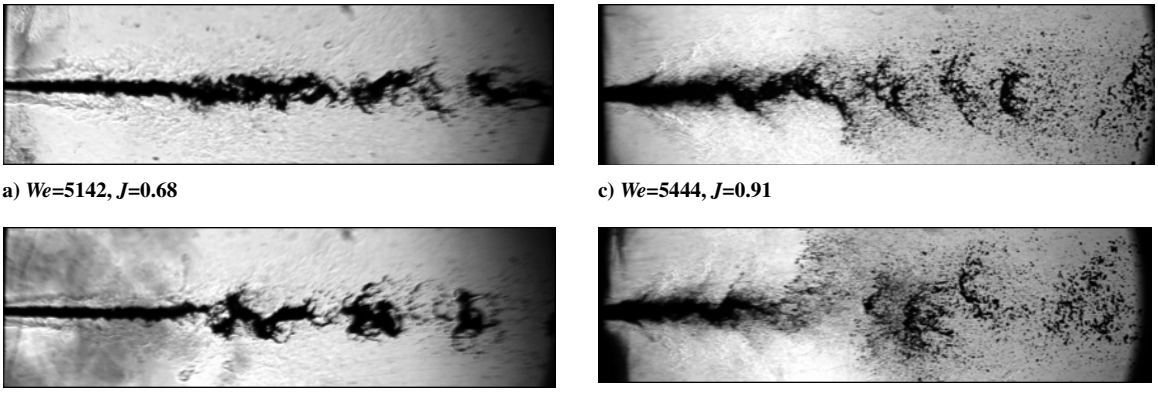

a) *We*=5142, *J*=0.68 c) *We*=5444, *J*=0.91

b) *We*=5014, *J*=1.46 d) *We*=8023, *J*=1.67

**Fig. 9 *J* effect at the Weber number around 5000 for a), b) $LOX/H_2$ tests, and c), d) $LOX/CH_4$ tests.**

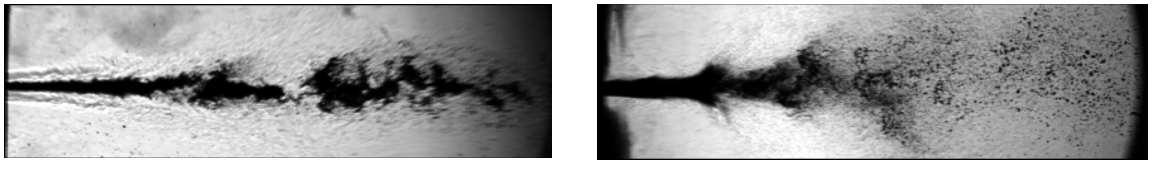

a) *We*=9844, *J*=1.28 b) *We*=9885, *J*=1.62

**Fig. 10 Comparison at the Weber number around 10,000 for a) $LOX/H_2$ test, and b) $LOX/CH_4$ test.**

Weber and *J* as supposed before, the atomization scenes should be similar at similar Weber and *J* conditions. What is found in the experiments is contrary to this, with the jet surface being much wavier, and more ligaments and droplets form around the wavy liquid core in $LOX/CH_4$ compared to $LOX/H_2$ tests. The dimensions of blobs and ligaments are smaller and droplets can be found at larger radial distances from the jet for $LOX/CH_4$. Larger amplitude of the lateral pulsation of the spray and earlier jet surface instability development results in shorter liquid intact core length in $CH_4$ sprays. These phenomena become more obvious with increasing Weber and *J* numbers and the spray shows dramatic differences especially at high Weber and *J* numbers as shown in Fig. 10. Test conditions for the images in Figs. 8–10 are listed in Table 3.

**Table 3 The detailed test conditions for images in Figs. 8–10**

| | Test | $D_l$, mm | $D_g$, mm | $We$ | $J$ | $u_g$, m/s | $u_l$, m/s | $Re_g$ | $Re_l$ | $\rho_g/\rho_l$ |
|---|---|---|---|---|---|---|---|---|---|---|
| $LOX/H_2$ | Figure 8a | 1.6 | 6.9 | 2208 | 0.30 | 226 | 8.2 | 138,200 | 56,200 | 3.9*e*-4 |
| | Figure 8b | 1.6 | 5.7 | 2461 | 0.73 | 235 | 5.5 | 105,600 | 37,500 | |
| | Figure 9a | | | 5142 | 0.68 | 340 | 8.2 | 152,800 | 56,200 | |
| | Figure 9b | 1.6 | 4.9 | 5014 | 1.46 | 333 | 5.5 | 113,400 | 37,500 | |
| | Figure 10a | | | 9844 | 1.28 | 467 | 8.2 | 159,000 | 56,200 | |
| $LOX/CH_4$ | Figure 8c | 1.4 | 6.9 | 1843 | 0.22 | 159 | 9.6 | 64,100 | 57,600 | 8.0*e*-4 |
| | Figure 8d | 1.6 | 5.7 | 2498 | 0.95 | 167 | 4.9 | 47,400 | 33,300 | |
| | Figure 9c | | | 5444 | 0.91 | 247 | 7.4 | 70,100 | 50,500 | |
| | Figure 9d | 1.6 | 5.0 | 8023 | 1.67 | 228 | 4.9 | 51,000 | 33,300 | |
| | Figure 10b | | | 9885 | 1.62 | 330 | 7.4 | 73,800 | 50,500 | |

Although the comparison of LOX-spray behavior in $LOX/H_2$ and $LOX/CH_4$ hot fire tests shows that with the presence of combustion, atomization becomes more complex and there must be other controlling parameters besides Weber and $J$, the two numbers still show their clear effects on atomization. In Figs. 8 and 9 the effect of the $J$ number at similar Weber number can be seen for a Weber number around 2000 in Fig. 8 and near to 5000 in Fig. 9. Higher gas/liquid momentum flux ratio $J$ has the tendency to promote jet instability and to result in an earlier onset of jet disintegration. This $J$ effect keeps working at different Weber conditions both in $H_2$ and $CH_4$ tests.

If Figs. 8b and 8d are compared with Figs. 9a and 9c, and Figs. 9b and 9d with Figs. 10a and 10b, respectively, the Weber effect can be seen at $J \approx 0.7$–$0.9$ and $J \approx 1.3$–$1.6$. As a ratio of aerodynamic and surface tension forces, the Weber number represents the relative disturbance of the gaseous coflow to the jet surface. With increasing Weber number, ligament and droplet dimensions become smaller and secondary atomization is augmented, especially shown in the images of $LOX/CH_4$ tests. The effect results in finer droplets at shorter downstream distance from the injector exit. Droplets are also transported to larger radial distances from the spray axis at higher Weber number, an effect particularly obvious in $LOX/CH_4$ tests. The very dark upstream region in Fig. 8d is due to water condensation on the optical windows, which has been processed to enhance the contrast of the region.

After this qualitative description of sprays in $LOX/H_2$ and $LOX/CH_4$ hot fire tests, a quantitative analysis is given to support the arguments above.

### 2. *LOX Intact Core Length*

Processing the shadowgraphs as described in Sec. III, the intact core lengths of the liquid oxygen sprays in $LOX/H_2$ and $LOX/CH_4$ hot fire tests at different injection conditions are determined and shown in Figs. 11a and 11b respectively. The $x$ axis represents $J$ number and the color bar shows a rough scale of the Weber number. The uncertainty of the values is about 20% for the $J$ number and about 10% for the Weber number.

The evaluated LOX intact core length presents a great variation even at very similar conditions. This is the reason why only a linear fit is given just to show the tendency of the effect of $J$. The standard deviation of the core length from the mean at a condition is also shown in Fig. 11. Considering the development of the jet instability as the reason of jet disintegration, it is reasonable to assume that the position of the primary disintegration point is pulsating with certain amplitude. What have been recorded in the images are different phases of jet pulsation and result in the variation of the intact core length during one test.

It is clearly seen that the LOX intact core length in $LOX/H_2$ tests are much longer than in $LOX/CH_4$ tests at similar Weber and $J$ conditions (more than 30% longer at $J < 0.5$ and 20% longer at $J = 1.5$). The results of Porcheron et al. [15] show the amplifying effect of gas/liquid density ratio on primary jet disintegration and a correlation is given as liquid core length $L/D_o \propto (\rho_g/\rho_l)^{-0.38}$ based on experimental results. This result gives an indication that the much higher density of $CH_4$ as compared to $H_2$ (see Tables 1 and 3) may be the reason of shorter intact core length for $CH_4$ tests even when injection conditions in terms of Weber and $J$ numbers are similar. The higher gaseous Reynolds numbers in $LOX/H_2$ tests seem to not promote the primary breakup of the LOX jet.

The mean intact core length is decreasing with increasing $J$ numbers. The Weber number does not show a similar obvious effect on the intact core length as $J$. At relative low Weber number ($We < \sim 5000$), the LOX core length in $H_2$ tests shows a slightly inverse relationship with Weber, but at high Weber the effect tends to diminish in both tests. The $J$ and Weber effects on intact core length have been found to be similar in $H_2$ and $CH_4$ tests.

The intact core length calculated from Eq. (1) of Lasheras et al. [4] and Eq. (2) of Davis [5] is compared with the core length measured in this work in Fig. 11. Results predicted by Lasheras are almost 1 order

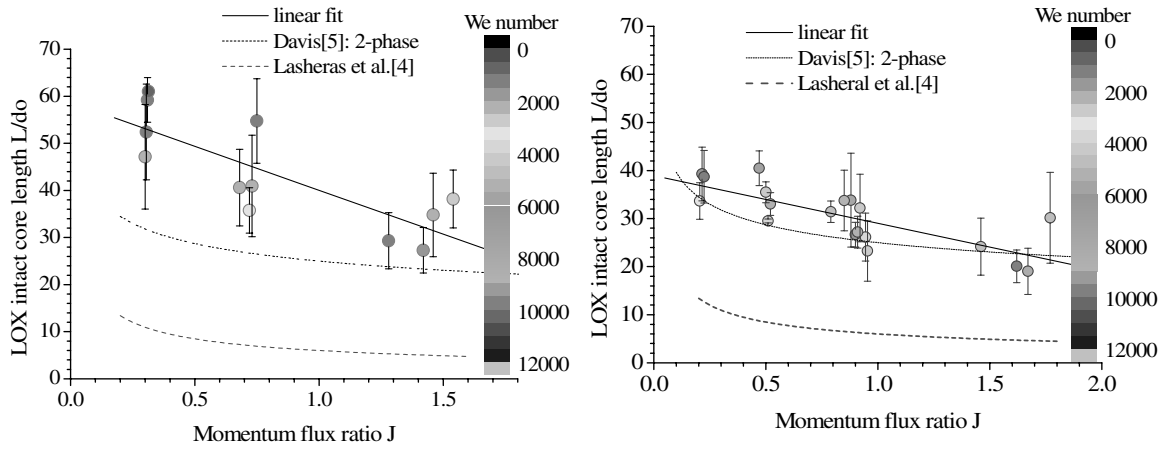


**a) $LOX/H_2$ tests** **b) $LOX/CH_4$ Tests**

**Fig. 11 $J$ and Weber effects on liquid intact core length with standard deviations.**

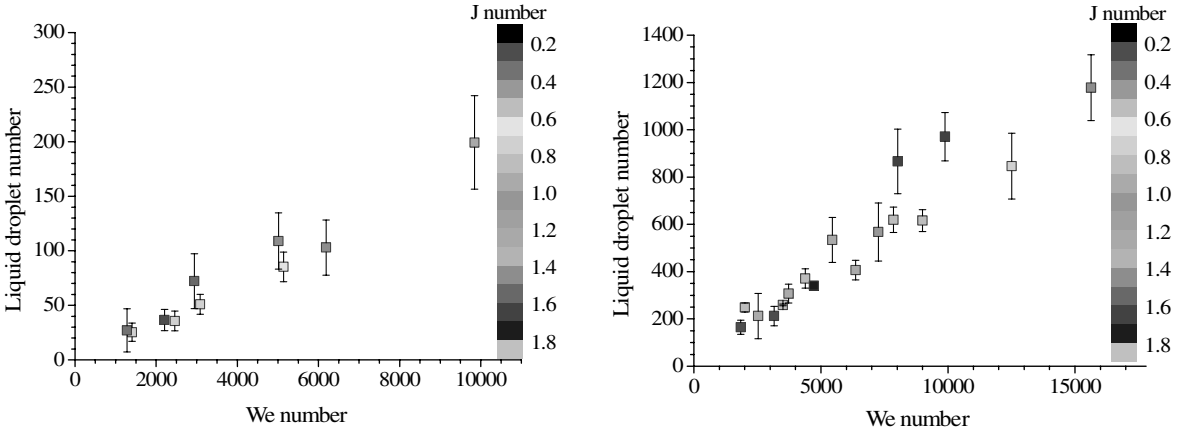


**a) LOX/$H_2$ tests** **b) LOX/$CH_4$ tests**

**Fig. 12 Weber and *J* effects on LOX-spray droplet numbers.**

shorter than the core lengths of Davis and this work. Davis's correlation is in good agreement with the LOX core length in the $CH_4$ hot tests.

*3. Droplet Numbers*

The evaluated droplet numbers of liquid oxygen sprays in LOX/$H_2$ and LOX/$CH_4$ hot fire tests are shown in Figs. 12a and 12b, respectively.

The Weber number is chosen as the *x* axis in Fig. 12; this is due to a strong relationship between the droplet number and Weber number with an alteration of the *J* having a small effect. The correlation of droplet number data with the Weber number is better than that of intact core length with *J* in Fig. 11. In the graphs it is clearly shown that more droplets and ligaments form and peel off a jet at higher Weber number both in the $H_2$ and $CH_4$ tests. According to Engelbert et al. [3], droplet formation is mainly characterized by the local Weber number. The result implies higher local Weber number at higher injection Weber due to the augment of bulk velocity in the chamber with increasing injection Weber number.

Considering liquid intact core length and droplet numbers as manifestations of primary breakup and secondary breakup, respectively, the effects of *J* and Weber numbers could be explained from the physical meanings of the two parameters. A high gas/liquid momentum flux ratio *J* at the injector exit means relative lower liquid jet inertia, which implies reduced tendency of the jet to resist changes. A jet with lower inertia is easier to disturb and shows an earlier onset of primary jet disintegration. The effect of the initial jet inertia almost fades away after the primary jet disruption and that is the reason why *J* has little effect on droplet numbers. The local Weber number controls secondary breakup and results in more and finer droplets. The quality of secondary breakup does not show a close relationship with the primary breakup length.

There is a notable difference of droplet numbers in the $H_2$ and $CH_4$ tests. The reason for lower droplet numbers in $H_2$ tests may be related to 1) the higher chemical reaction rate for LOX/H2 resulting in more consumption of gaseous oxygen and thus the partial pressure gradient of gaseous $O_2$ is increased. This should enhance the evaporation rate of liquid oxygen. 2) The higher rate of chemical heat release promotes the evaporation of oxygen droplets.

The clear effects of Weber and *J* numbers on LOX sprays and the great differences between LOX/$H_2$ and LOX/$CH_4$ sprays in hot test implies the significant influence of combustion properties on atomization behavior.

## B. Flame

*1. Flame Anchoring*

As described in Sec. III, the OH emission within the reaction zone was recorded to obtain quantitative information on the flame patterns. Comparing LOX/$H_2$ and LOX/$CH_4$ flames it is found that LOX/$H_2$ flames are always attached to the injector rim, whereas LOX/$CH_4$ flames are easily lifted off under the conditions tested in this work. The distance of the flame base position to the injector face plate can be 8 times the LOX-post diameter for the case in Fig. 13d.

Flame stabilization in the turbulent two-phase flow depends on many factors. The primary reason for the liftoff potential of $CH_4$ flame is the much slower kinetics compared with $H_2$ (see Table 1).

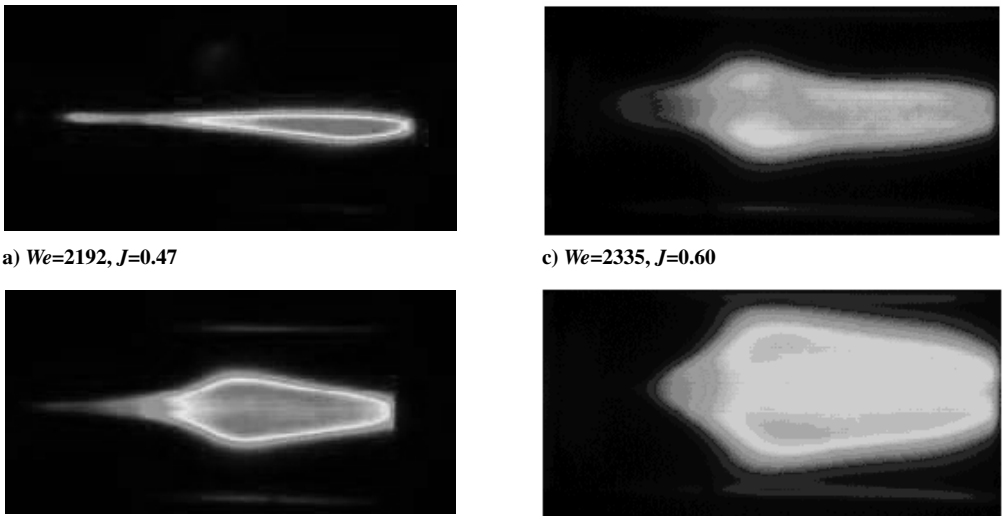

**a) *We*=2192, *J*=0.47** **c) *We*=2335, *J*=0.60**

**b) *We*=7007 *J*=0.65** **d) *We*=7936, *J*=0.56**

**Fig. 13 Weber effect on LOX/$CH_4$-spray flame for a), b) LOX/$H_2$ tests, and c), d) LOX/$CH_4$ tests.**

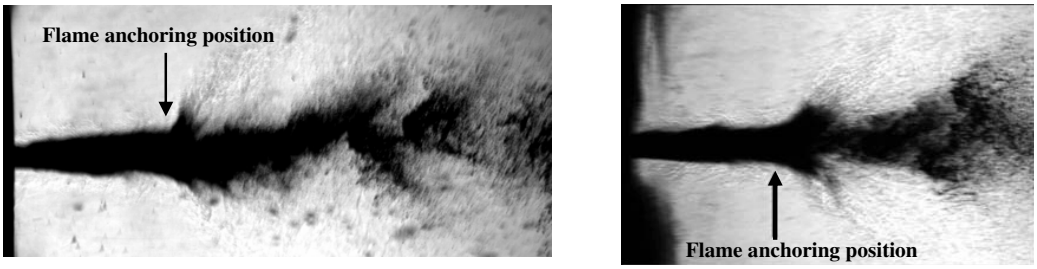


a) *We*=7936, *J*=0.56 b) *We*=9885, *J*=1.65

**Fig. 14 Detail of the spray pattern near the flame liftoff position of LOX/$CH_4$-spray flames.**

Figure 13 shows as an example the different flame patterns for the two propellant pairs under similar Weber and *J* combinations.

Lifted flames give their fingerprint also in the shadowgraph images. For the lifted flames a distinct change in the spray pattern has been observed at the flame anchoring position marked by the arrows in Fig. 14. Upstream of the anchoring position the spray is rather confined in a small angle and few isolated liquid fibers and droplets are visible. At the anchoring position a sudden increase of the spreading angle of the spray is observed. The sudden expansion of the spray may be due to the rapid reactive heat release starting from the anchoring point. This clearly demonstrates the influence of the flame anchoring mechanism on the spray pattern.

No significant correlation of the liftoff distance with the nondimensional numbers Weber and *J* has been found. Although one would expect that the liftoff distance is increasing with increasing $CH_4$ velocity and thus with increasing Weber number, this seems not to be the case in our results.

### 2. *Flame Angle*

The dependence of the flame angles for LOX/$CH_4$ and LOX/$H_2$ spray flames on the Weber number is shown in Fig. 15. A comparison of the results for both propellants shows increasing Weber-number results in an increasing flame spreading angle. The methane data shown in the graph can be separated into two groups: one for lifted flames and the other for attached flames. Lifted flames have only been observed for methane and flame angles of lifted are much broader than for attached LOX/$CH_4$ flames. For attached flames similar results are observed for LOX/$H_2$ and $CH_4$.

The Weber dependence of the flame angle is in agreement with the observed Weber dependence of droplet numbers and the radial dispersion of droplets. Unlike for Weber number, no significant correlation of the flame angle with either the momentum flux ratio or the velocity ratio has been found. It is worth noticing that the flame angles in single-injector experiments may be broader than flame angles from multi-injectors tests since there is no confinement by other streamlines from neighboring injectors.

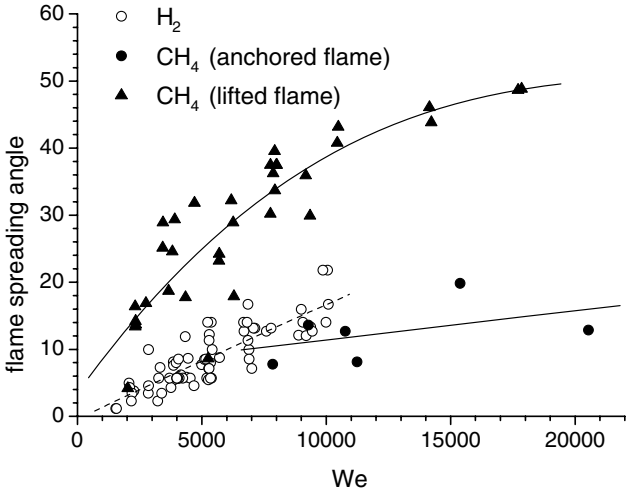


**Fig. 15 Flame spreading angle vs Weber number for LOX/$CH_4$ and LOX/$H_2$ tests.**

## V. Summary and Conclusions

By comparing LOX/$H_2$ and LOX/$CH_4$ spray combustion phenomenology, significant differences of the sprays and flames have been observed for similar injection conditions as defined by Weber number and momentum flux ratio.

Compared to sprays of LOX/$H_2$ for hot fire tests, LOX/$CH_4$ sprays present shorter liquid oxygen core length, more discernible droplets, and larger spray dispersion at similar injection Weber and *J* numbers.

The effect of *J* and Weber numbers on atomization in hot fire tests is similar to the findings under cold-flow conditions: the *J* number mainly governs the primary breakup of the liquid jet and thus determines the liquid core length, and the Weber number mainly influences secondary atomization and flame angles.

Anchored LOX/$CH_4$ flames show similar flame angles as anchored LOX/$H_2$ flames. Lifted flames are only observed for LOX/$CH_4$ and these flames show larger flame angles as the attached flames. This together with the data from the spray visualizations proves the strong coupling between flame stabilization process, flame characteristics, and atomization.

From the results obtained until now, it is obvious that nondimensional numbers characterizing the fluid-dynamic interaction of the two fluids at the injector exit are not sufficient to scale coaxial injector performance in hot fire tests from one fuel to another. At identical injection conditions in terms of Weber number and momentum flux ratio, especially the flame stabilization mechanisms may be different for different fuels. Scaling of injector designs for different types of fuel has therefore to take into account kinetic and transport properties associated with combustion.

## Acknowledgments

The support of Avio S.P.A. to F. Cuoco and of the China Scholarship Council to B. Yang is gratefully acknowledged.

## References

[1] Ledoux, M., Caré, I., Micci, M., Glogowski, M., Vingert, L., and Gicquel, P., "Atomization of Coaxial Injectors," *Proceedings of the 2nd International Symposium on Liquid Rocket Propulsion*, ONERA, Châtillon, France, 1995, pp. 2-1–2-19.

[2] Farago, Z., and Chigier, N., "Morphological Classification of Disintegration of Round Liquid Jets," *Atomization and Sprays*, Vol. 2, No. 2, 1992, pp. 137–153.

[3] Engelbert, C., Hardalupas, Y., and Whitelaw, J. H., "Breakup Phenomena in Coaxial Airblast Atomizer," *Proceedings of the Royal Society of London A*, Vol. 451, No. 1941, 1995, pp. 189–229.

[4] Lasheras, J. C., Villermaux, E., and Hopfinger, E. J., "Break-Up and Atomization of a Round Water Jet by a High-Speed Annular Air Jet," *Journal of Fluid Mechanics*, Vol. 357, Feb. 1998, pp. 351–379.

[5] Davis, D, W., and Chehroudi, B., "Measurements in an Acoustically Driven Coaxial Jet Under Sub-, Near-, and Supercritical Conditions," *Journal of Propulsion and Power*, Vol. 23, No. 2, 2007, pp. 364–374.

[6] Woodward, R. D., Pal, S., Farhangi, S., and Santoro, R. J., "LOX/GH2 Shear Coaxial Injector Atomization Studies at Large Momentum Flux Ratios," AIAA Paper 2006-5203, 2006.
[7] Wanhainen, J. P., Parish, H. C., and Conrad, E. W., "Effect of Propellant Injection Velocity on Screech in 20000 Pound Hydrogen-Oxygen Rocket Engine," NASA TN D-3373, 1966.
[8] Smith, J. J., Schneider, G., Suslov, D., Oschwald, M., and Haidn, O., "Steady-State High Pressure LOx/H2 Rocket Engine Combustion," *Aerospace Science and Technology*, Vol. 11, No. 1, 2007, pp. 39–47.
[9] Levebre, A. H., *Atomization and Sprays*, Taylor and Francis, London, 1989.
[10] Chigier, N., and Reitz, R. D., "Regines of Jet Breakup and Breakup Mechanisms (Physical Aspects)," *Recent Advances in Spray Combustion: Spray Atomization and Drop Burning Phenomena*, edited by K. Kuo, Vol. 166, Progress in Astronautics and Aeronautics, AIAA, Washington, D.C., 1995, pp. 109–135.
[11] Eroglu, H., and Chigier, N., "Wave Characteristics of Liquid Jets from Airblast Coaxial Atomizers," *Atomization and Sprays*, Vol. 2, No. 3, 1992, pp. 295–318.
[12] Rahman, S. A., and Santoro, R. J., "A Review of Coaxial Gas/Liquid Spray Experiments and Correlations," AIAA Paper 94-2772, 1994.
[13] Villermaux, E., "Mixing and Spray Formation in Coaxial Jets," *Journal of Propulsion and Power*, Vol. 14, No. 5, 1998, pp. 807–817.
[14] Hardalupas, Y., and Whitelaw, J. H., "Characteristics of Sprays Produced by Coaxial Airblast Atomizers," *Journal of Propulsion and Power*, Vol. 10, No. 4, 1994, pp. 453–460.
[15] Porcheron, E., Carreau, J. L., Prevost, L., Le Visage, D., and Roger, F., "Effect of Injection Gas Density on Coaxial Liquid Jet Atomization," *Atomization and Sprays*, Vol. 12, Nos. 1–3, 2002, pp. 209–227.
[16] Vingert, L., Gicquel, P., Lourme, D., and Ménoret, L., "Coaxial Injector Atomization," *Liquid Rocket Combustion Instability*, edited by V. Yang, Vol. 169, Progress in Astronautics and Aeronautics, AIAA, Washington, D.C., 1995, pp. 145–189.
[17] Mayer, W., Ivancic, B., Schik, A., and Hornung, U., "Propellant Atomization in LOX/GH2 Rocket Combustors," *34nd AIAA/ASME/SAE/ASEE Jet Propulsion Conference and Exhibit*, AIAA, Reston, VA, July 13–15, 1998; also AIAA Paper 1998–3685.
[18] Mayer, W., and Smith, J., "Fundamentals of Supercritical Mixing and Combustion of Cryogenic Propellants," *Liquid Rocket Thrust Chambers: Aspects of Modeling, Analysis and Design*, edited by V. Yang, Vol. 200, Progress in Aeronautics and Astronautics, AIAA, Reston, VA, 2004, pp. 339–367.
[19] Herding, G., Snyder, R., Scouflaire, P., Rolon, C., and Candel, S., "Flame Stabilization in Cryogenic Propellant Combustion," *Proceedings of the 26th Symposium (International) on Combustion*, The Combustion Institute, Pittsburg, PA, 1996, pp. 2041–2047.
[20] Candel, S., Herding, G., Synder, R., Scouflaire, P., Rolon, C., Vingert, L., Habiballah, M., Grisch, F., Péalat, M., Bouchardy, P., Stepowski, D., Cessou, A. and Colin, P., "Experimental Investigation of Shear Coaxial Cryogenic Jet Flames," *Journal of Propulsion and Power*, Vol. 14, No. 5, 1998, pp. 826–834.
[21] Juniper, M., and Candel, S., "Edge Diffusion Flame Stabilization Behind a Step over a Liquid Reactant," *Journal of Propulsion and Power*, Vol. 19, No. 3, 2003, pp. 332–341.
[22] Younglove, B. A., "Thermo-Physical Properties of Fluids. 1," *Journal of Physical and Chemical Reference Data*, Vol. 11, Suppl. 1, 1982, pp. 97–161.
[23] Younglove, B. A., and Ely, J. F., "Thermo-Physical Properties of Fluids. 2," *Journal of Physical and Chemical Reference Data*, Vol. 16, No. 4, 1987, pp. 577–798.
[24] Fiock, E. F., *High Speed Aerodynamics and Jet Propulsion, Vol. 9: Physical Measurements in Gas Dynamics and Combustion, Sec. K: Measurement of Burning Velocity*, Princeton Univ. Press, Princeton, NJ, 1953, pp. 409–438.
[25] Coward, H. F., and Jones, G. W., *Limits of Flammability of Gases and Vapors*, Bulletin 503, Bureau of Mines, 1952.
[26] Turns, S. R., *An Introduction to Combustion: Concepts and Applications*, 2nd ed., McGraw–Hill, New York, 2000.

D. Talley
*Associate Editor*